A regulatory feedback loop involving p63 and IRF6 links the pathogenesis of 2 genetically different human ectodermal dysplasias

Francesca Moretti, … , Luisa Guerrini, Antonio Costanzo

Research Article

The human congenital syndromes ectrodactyly ectodermal dysplasia-cleft lip/palate syndrome, ankyloblepharon ectodermal dysplasia clefting, and split-hand/foot malformation are all characterized by ectodermal dysplasia, limb malformations, and cleft lip/palate. These phenotypic features are a result of an imbalance between the proliferation and differentiation of precursor cells during development of ectoderm-derived structures. Mutations in the *p63* and interferon regulatory factor 6 (*IRF6*) genes have been found in human patients with these syndromes, consistent with phenotypes. Here, we used human and mouse primary keratinocytes and mouse models to investigate the role of p63 and IRF6 in proliferation and differentiation. We report that the ΔNp63 isoform of p63 activated transcription of *IRF6*, and this, in turn, induced proteasome-mediated ΔNp63 degradation. This feedback regulatory loop allowed keratinocytes to exit the cell cycle, thereby limiting their ability to proliferate. Importantly, mutations in either *p63* or *IRF6* resulted in disruption of this regulatory loop: *p63* mutations causing ectodermal dysplasias were unable to activate *IRF6* transcription, and mice with mutated or null *p63* showed reduced *Irf6* expression in their palate and ectoderm. These results identify what we believe to be a novel mechanism that regulates the proliferation-differentiation balance of keratinocytes essential for palate fusion and skin differentiation and links the pathogenesis of 2 genetically different groups of ectodermal dysplasia syndromes into a common molecular pathway.

Find the latest version:

https://jci.me/40267/pdf

A regulatory feedback loop involving p63 and IRF6 links the pathogenesis of 2 genetically different human ectodermal dysplasias

Francesca Moretti,[1] Barbara Marinari,[1] Nadia Lo Iacono,[2] Elisabetta Botti,[1] Alessandro Giunta,[1] Giulia Spallone,[1] Giulia Garaffo,[3] Emma Vernersson-Lindahl,[4] Giorgio Merlo,[3] Alea A. Mills,[4] Costanza Ballarò,[5] Stefano Alemà,[5] Sergio Chimenti,[1] Luisa Guerrini,[2] and Antonio Costanzo[1,6]

[1]Department of Dermatology, University of Rome "Tor Vergata," Rome, Italy. [2]Department of Biomolecular Science and Biotechnology, University of Milan, Milan, Italy. [3]Dulbecco Telethon Institute, Molecular Biotechnology Center University of Torino, Torino, Italy. [4]Cold Spring Harbor Laboratory, Cold Spring Harbor, New York, USA. [5]Istituto di Biologia Cellulare, Consiglio Nazionale delle Ricerche, Monterotondo Scalo, Rome, Italy. [6]Rome Oncogenomic Centre, Via Elio Chianesi, Rome, Italy.

The human congenital syndromes ectrodactyly ectodermal dysplasia-cleft lip/palate syndrome, ankyloblepharon ectodermal dysplasia clefting, and split-hand/foot malformation are all characterized by ectodermal dysplasia, limb malformations, and cleft lip/palate. These phenotypic features are a result of an imbalance between the proliferation and differentiation of precursor cells during development of ectoderm-derived structures. Mutations in the *p63* and interferon regulatory factor 6 (*IRF6*) genes have been found in human patients with these syndromes, consistent with phenotypes. Here, we used human and mouse primary keratinocytes and mouse models to investigate the role of p63 and IRF6 in proliferation and differentiation. We report that the ΔNp63 isoform of p63 activated transcription of *IRF6*, and this, in turn, induced proteasome-mediated ΔNp63 degradation. This feedback regulatory loop allowed keratinocytes to exit the cell cycle, thereby limiting their ability to proliferate. Importantly, mutations in either *p63* or *IRF6* resulted in disruption of this regulatory loop: *p63* mutations causing ectodermal dysplasias were unable to activate *IRF6* transcription, and mice with mutated or null *p63* showed reduced *Irf6* expression in their palate and ectoderm. These results identify what we believe to be a novel mechanism that regulates the proliferation-differentiation balance of keratinocytes essential for palate fusion and skin differentiation and links the pathogenesis of 2 genetically different groups of ectodermal dysplasia syndromes into a common molecular pathway.

Introduction

The p53-related transcriptional activator p63 is expressed in basal cells of stratified epithelia, in myoepithelial cells of the breast and salivary glands, and in the proliferative compartment of gastric mucosa (1, 2). As a result of the alternative usage of 2 promoters and of complex alternative splicing, the *p63* gene encodes 6 isoforms (1). Of these, the transactivation (TA) isoforms contain an N-terminal TA domain, which is absent in the ΔN isoforms (1). In ΔNp63 isoforms, an additional TA domain has been recognized in the C terminus, which is responsible for ΔN-specific transcriptional activities distinct from that of TA isoforms (3, 4). ΔNp63 isoforms are expressed in cells of stratified epithelia and contribute to the regulation of the proliferative potential of epithelial stem cells and to epidermal morphogenesis (5–7). The critical role for p63 in regulating epidermal morphogenesis is illustrated by the phenotype of *p63*−/− mice, which fail to develop an epidermis, other stratified epithelia, and epithelial appendages (2, 8). The single layer of epithelial cells covering *p63*−/− mice at birth fails to provide barrier function, resulting in early postnatal lethality due to severe dehydration.

Mutations in the *p63* gene are found in a number of dominantly inherited human congenital disorders, including ectrodactyly ectodermal dysplasia-cleft lip/palate syndrome (EEC), ankyloblepharon ectodermal dysplasia clefting (AEC), and nonsyndromic split-hand/foot

malformation (SHFM) (9, 10). These syndromes share several phenotypic features, consisting of ectodermal dysplasia, limb malformations, and cleft lip/palate, that can be related to alterations of a tightly controlled balance between proliferation and differentiation of precursor cells during the development of ectoderm-derived epithelia and organs (10). Since p63 is a transcription factor, the molecular basis of these defects most likely resides in the inability of mutated p63 proteins to properly activate/repress expression of target genes, which are beginning to be identified. Indeed, phenotypic defects found in p63-linked ectodermal dysplasias are common to other congenital syndromes caused by mutation in p63 target genes, such as the *DLX* genes, whose mutation/misregulation is associated with SHFMI (*DLX5* and *DLX6*) (11) or with the trichodentoosseous syndrome (*DLX3*) (12), or Claudin-1, whose mutation leads to the NISCH syndrome (13). Interferon regulatory factor 6 (*IRF6*) is a member of a conserved family of IFN-dependent transcription factors known to regulate the proliferation-differentiation switch in epidermal cells and shown to be required for palate closure during embryonic development (14–16). Mutations in this gene cause the van der Woude and the popliteal pterygium syndromes (17), conditions resembling p63-linked ectodermal dysplasias in many aspects (10).

Here we show that *IRF6* is a p63 transcriptional target that limits keratinocyte proliferation by inducing ΔNp63 proteasome-mediated degradation. Mutations in *p63* or *IRF6* disrupt this regulatory loop, altering the critical balance between differentiation and proliferation during development, leading to clinically evident defects.
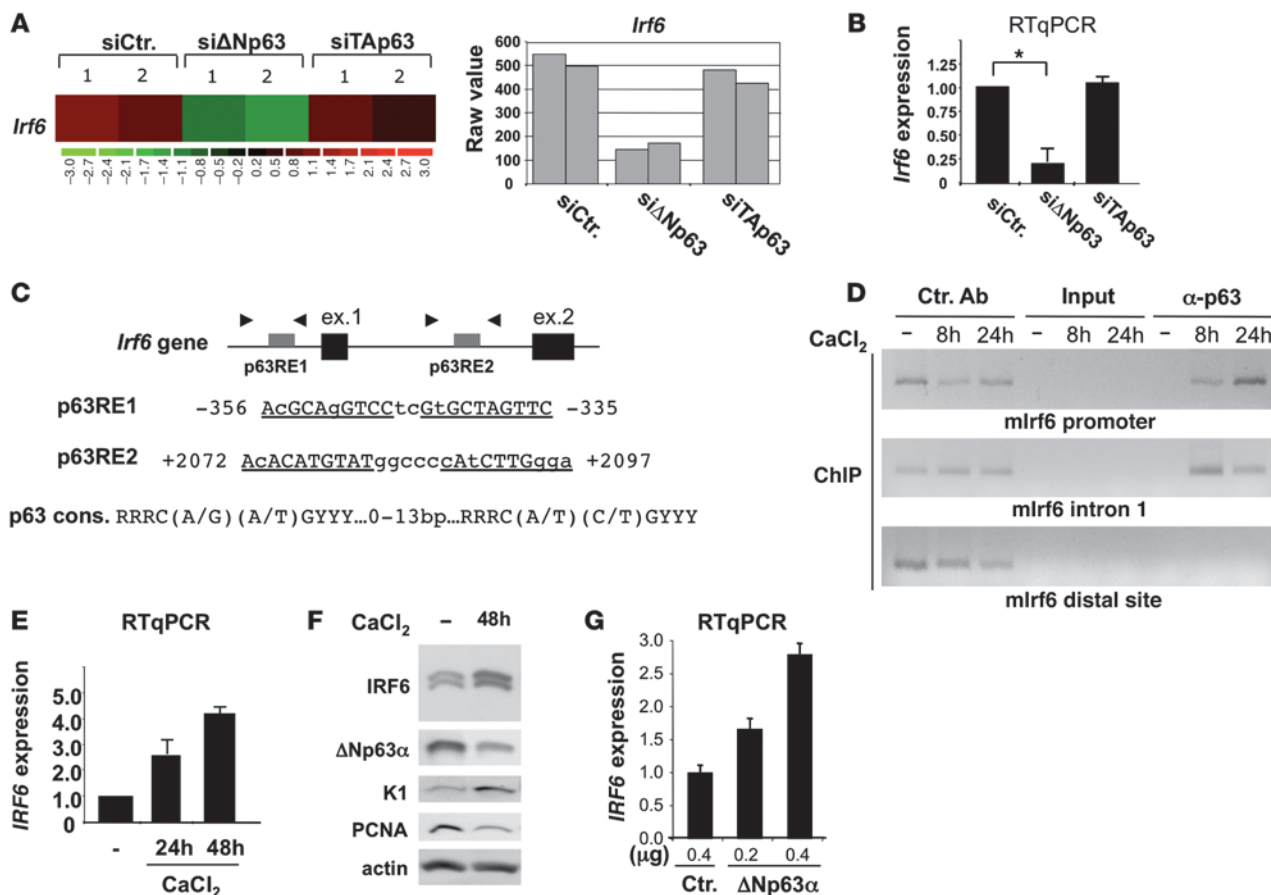
Figure 1

Irf6 is a direct p63 target. (**A**) Microarray analysis of *Irf6* RNA expression in mouse primary keratinocytes transfected with ΔNp63- or TAp63-specific siRNAs. Representative heat map and raw value data are shown. (**B**) *Irf6* mRNA expression in mouse primary keratinocytes transfected with ΔNp63- or TAp63-specific siRNA. Data are presented as mean ± SEM. *P = 0.001. (**C**) p63 REs present within the *Irf6* gene. The p63 RE consensus sequence is shown at the bottom. Arrowheads indicate the position of primers used in ChIP analysis. Putative p53/p63 REs were identified by PathSearch algorithm. (**D**) ChIP analysis to detect p63 occupying the *Irf6* promoter in differentiating mouse primary keratinocytes. PCR was performed using the indicated primers (Supplemental Methods). (**E**) *IRF6* expression in human primary keratinocytes by RT-qPCR. Data are presented as mean ± SEM. (**F**) Immunoblot analysis of human primary keratinocyte protein extracts to detect IRF6, ΔNp63, K1, and PCNA proteins. (**G**) *IRF6* expression in human primary keratinocytes transfected with the indicated expression vectors and induced to differentiate. ΔNp63α induces *IRF6* mRNA. Data are presented as mean ± SEM. cons., consensus sequence; ex., exon; mIrf6, mouse Irf6; siCtr., control siRNA; siΔNp63, ΔNp63-specific siRNA; siTAp63, TAp63-specific siRNA.

Results

Irf6 is a direct ΔNp63 target gene. In order to identify genes specifically regulated by TAp63 or ΔNp63, we performed transcriptional profiling of primary mouse keratinocytes, in which TAp63 or ΔNp63 were selectively depleted by siRNA (13) (Supplemental Figure 1, A and B; supplemental material available online with this article; doi:10.1172/JCI40267DS1). In addition to known p63 targets (e.g., scotin, stratifin) (Supplemental Table 1), we identified *Irf6* as a positively regulated target in ΔNp63-depleted cells but not in TAp63-depleted cells (Figure 1, A and B).

Using ChIP assays, we determined that endogenous *Irf6* is a direct p63 target in keratinocytes. We identified 2 p63-like consensus binding sites upstream of the transcription initiation site and in the first *Irf6* intron (Figure 1C); both sites directly interact with p63 during calcium-induced differentiation of primary mouse keratinocytes (Figure 1D). Binding of p63 onto these *Irf6* responsive elements (REs) precedes a marked increase in *Irf6* mRNA and Irf6 protein levels

(Figure 1, E and F); moreover, exogenously expressed ΔNp63 increased *Irf6* transcript levels (Figure 1G) and induced a reporter gene driven by an *Irf6* promoter (Supplemental Figure 1C). In contrast, an *Irf6* promoter, with the RE mutated so that it could not bind ΔNp63 in oligo pull-down experiments, was activated to a lesser degree by exogenously expressed ΔNp63 (Supplemental Figure 1, C and D).

p63 is required for Irf6 expression in vivo. To determine whether *Irf6* expression is p63-dependent in vivo, we examined the distribution of *Irf6* mRNA using in situ hybridization on sections from wild-type and *p63⁻/⁻* mice (8). As expected, the palatal and tooth epithelia of *p63⁻/⁻* embryos displayed reduced expression of *Irf6* compared with the heterozygous or wild-type embryos. Expression of the mesenchymal marker *Msx1* was not significantly changed (Figure 2A), demonstrating the correspondence of the anatomical structures and indicating that the initial steps of their morphogenesis were normally induced (18). Reduction of *Irf6* expression was confirmed by real-time quantitative PCR (qPCR), performed on *p63⁻/⁻* embryonic ectoderm (Figure 2B).
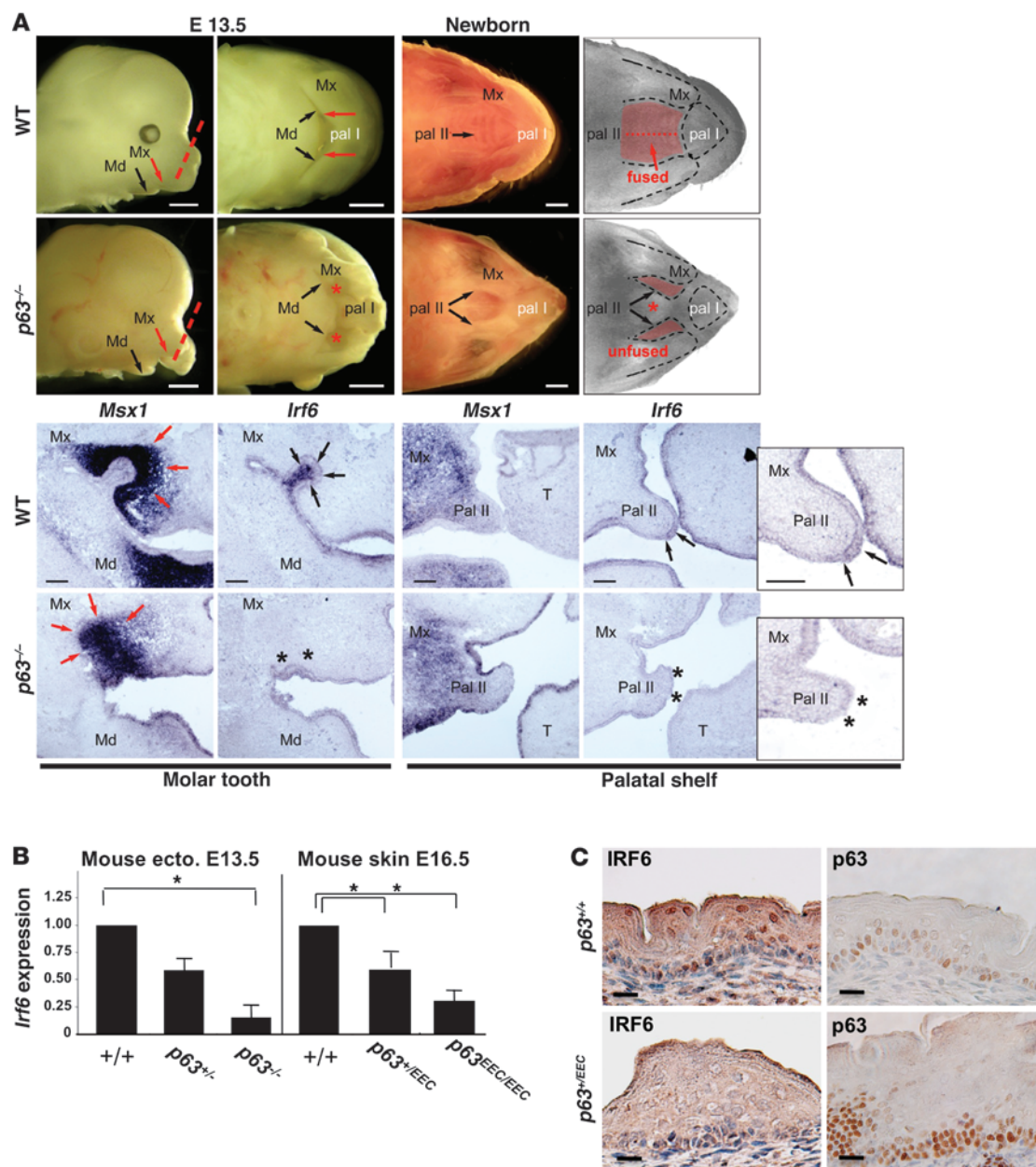
Figure 2
p63 is required for *Irf6* expression in vivo. (**A**) The palatal phenotype in E13.5 and newborn *p63*^{−/−} embryos. The age is indicated at the top columns, and genotypes are reported to the left of rows. The images on the far right of each row illustrate the newborn specimens, after removal of the mandible (Md). The dashed black lines define the profile of the anatomical structures. In *p63*^{−/−} embryos, the maxillae (Mx) and the secondary palate (pal II) fail to fuse with the primary palate (pal I) and the secondary palate fails to fuse on the midline (thin dashed red line, red asterisks). In situ hybridization for *Msx1* and *Irf6* on coronal sections of the tooth (E13.5, left) and palatal (E13.5, right) region of wild-type and *p63*^{−/−} embryos. The section plane is indicated by thick dashed red lines. Expression of *Msx1* is indicated with red arrows. Expression of *Irf6* is reduced in the tooth and palate epithelia of the *p63*^{−/−} specimen (black arrows and asterisks for wild-type and mutant, respectively). Scale bars: 1 mm (white); 50 μm (black). T, tongue. (**B**) RT-qPCR analysis of *Irf6* mRNA in ectoderm of *p63*^{−/−} mice aged E13.5 and EEC mice aged E16.5. The wild-type value is set as 1. Data are presented as mean ± SEM. *$P = 0.01$. (**C**) Skin sections from E16.5 wild-type (+/+) or *p63*[+/EEC] knock-in mice, immunostained with Irf6- or p63-specific antibodies. Irf6 immunostaining is strongly reduced in *p63*[+/EEC] mice, while p63 expression is increased. Images are representative of data obtained from 3 littermates for each genotype. Scale bars: 30 μm.

We also determined *Irf6* mRNA expression levels in mouse embryos containing the knock-in *p63* mutation R279H (found in EEC patients) at various developmental ages. Animals homozygous for this mutation were very similar to the null ones, in terms of skin, limb, and craniofacial defects, and displayed reduced *Irf6* mRNA expression in the epidermis (Figure 2B) and in the tooth and palate epithelia (data not shown). Interestingly, animals heterozygous for this mutation show a low-penetrance, EEC-related phenotypic
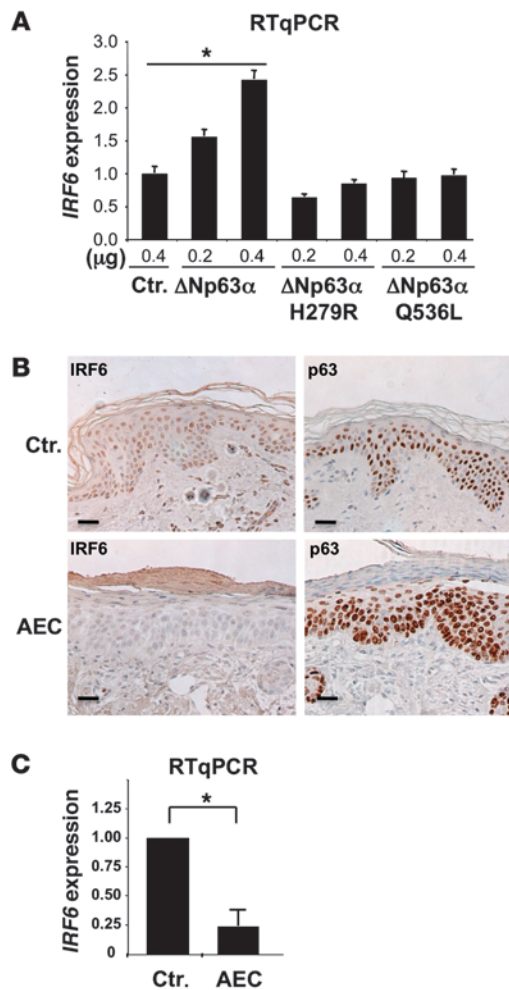
Figure 3
p63 mutations affect IRF6 expression in vitro and in vivo. (**A**) *IRF6* expression in H1299 cells transfected with ΔNp63α (WT), ΔNp63α H279R (EEC), and ΔNp63α Q536L (AEC) expression vectors. Data are presented as mean ± SEM. *P = 0.01. (**B**) Skin sections from a newborn affected by AEC syndrome or from normal subjects (Ctr), immunostained with IRF6- and p63-specific antibodies. IRF6 expression is strongly downregulated in AEC epidermis. Images are representative of data obtained from 3 unrelated normal subjects and from 3 independent sections from the AEC patient. Scale bars: 30 μm. (**C**) RT-qPCR showing *IRF6* mRNA downregulation in total RNA extracted from formalin-fixed, paraffin-embedded sections. Results were normalized against hARP. Data are presented as mean ± SEM. *P = 0.001.

spectrum, including cleft palate and ectrodactyly, that more closely resembles the human EEC syndrome than that of *p63*-null mice (ref. 19 and A.A. Mills et al., unpublished observations). The skin of *p63*[+/EEC] embryos (Figure 2C) and newborns showed patches of hyperproliferating epidermis; in these patches, IHC staining revealed a marked reduction of Irf6 nuclear expression, as compared with the epidermis of wild-type mice (Figure 2C, left), and a marked increase in p63 nuclear expression (Figure 2C, right). Consistently, exogenous expression of ΔNp63s carrying either the R279H or the Q536L mutations (the latter associated to the AEC syndrome) in human keratinocytes resulted in a reduced *IRF6* expression compared with wild-type ΔNp63 (Figure 3A). These findings were

extended to human skin by examining IRF6 expression in biopsies from an AEC patient (carrying *p63* I537T mutation) (13, 20). As shown in Figure 3B, the AEC epidermis was parakeratotic and displayed strong reduction in IRF6 immunoreactivity as compared with normal skin, also confirmed at the mRNA level (Figure 3C). This observation correlated with abnormally high levels of p63, ectopically detected in the upper epidermal layers, including the flattened cells of intermediate zone between the spinous layer and the parakeratotic stratum corneum (Figure 3B).

IRF6 induces downregulation of ΔNp63 in human keratinocytes. The developmental defects observed in *Irf6* mutant mice are thought to result from the inability of *Irf6* mutant cells to exit the cell cycle, leading to an undifferentiated hyperproliferative epidermis (14, 15). In addition, mice heterozygous for *p63* and the *Irf6* mutation R84C display cleft of the secondary palate, as the medial edge epithelial cells fail to undergo their normal differentiation program (21). In this regard, ΔNp63 is a key regulator of epithelial cell proliferative potential and is upregulated in the epidermis of *Irf6* mutant mice (14, 15). We also noted a reciprocal relationship between IRF6 and p63 protein expression during calcium-induced differentiation of human primary keratinocytes (Figure 1F) and in immunofluorescence experiments performed on normal human epidermis (Supplemental Figure 2). Therefore, we reasoned that, following the initial activation of *IRF6* expression by ΔNp63, IRF6 then promotes the downregulation of ΔNp63, and that this regulation might favor the exit of keratinocytes from the cell cycle. To test this hypothesis, we exogenously expressed IRF6 in normal keratinocytes and analyzed the endogenous expression of ΔNp63. The results indicate that IRF6-overexpressing cells display reduced levels of ΔNp63 (Figure 4A and Table 1).

Accordingly, Δ*Np63* mRNA and protein expression is markedly reduced during keratinocyte differentiation (1, 22). To evaluate the possible role of *IRF6* in differentiation-induced ΔNp63 downregulation, we depleted IRF6 in human primary keratinocytes using siRNA. We observed that, in IRF6-depleted proliferating keratinocytes, the amount of ΔNp63α was similar to that in control cells, whereas differentiating keratinocytes failed to induce full ΔNp63 downregulation and also displayed higher levels of the proliferation marker PCNA (Figure 4B). IRF6 depletion caused inhibition of terminal differentiation, as observed by reduced levels of loricrin (*LOR*) mRNA in differentiating IRF6-depleted cells (Supplemental Figure 3, A and B).

Downregulation of ΔNp63 during keratinocyte differentiation is due, at least in part, to the expression of a specific miRNA (miR203) (23, 24). However, siRNA-mediated depletion of IRF6 had no significant effect on miR203 expression, indicating that IRF6 is unlikely to be involved in this mechanism (Supplemental Figure 3C). An alternative means to downregulate ΔNp63 expression is by proteasome-mediated degradation (25, 26), and indeed, we found that IRF6-induced ΔNp63 protein degradation was mediated by the proteasome, being blocked by treatment with the specific inhibitor MG132 (Figure 4C), which does not affect exogenous Δ*Np63* mRNA level (Supplemental Figure 3D). Thus, IRF6 targets ΔNp63α and ΔNp63β isoforms for degradation but not ΔNp63γ or TAp63α isoforms (Supplemental Figure 4).

In addition to altered transcriptional properties, mutated ΔNp63 might also have different sensitivity to IRF6-dependent downregulation. We therefore tested the effect of IRF6 overexpression on the stability of the ΔNp63-R279H (EEC mutant) protein and found that this mutant is resistant to IRF6-mediated downregulation (Figure 4D). Conversely, *IRF6* mutant R84C, a mutation causing
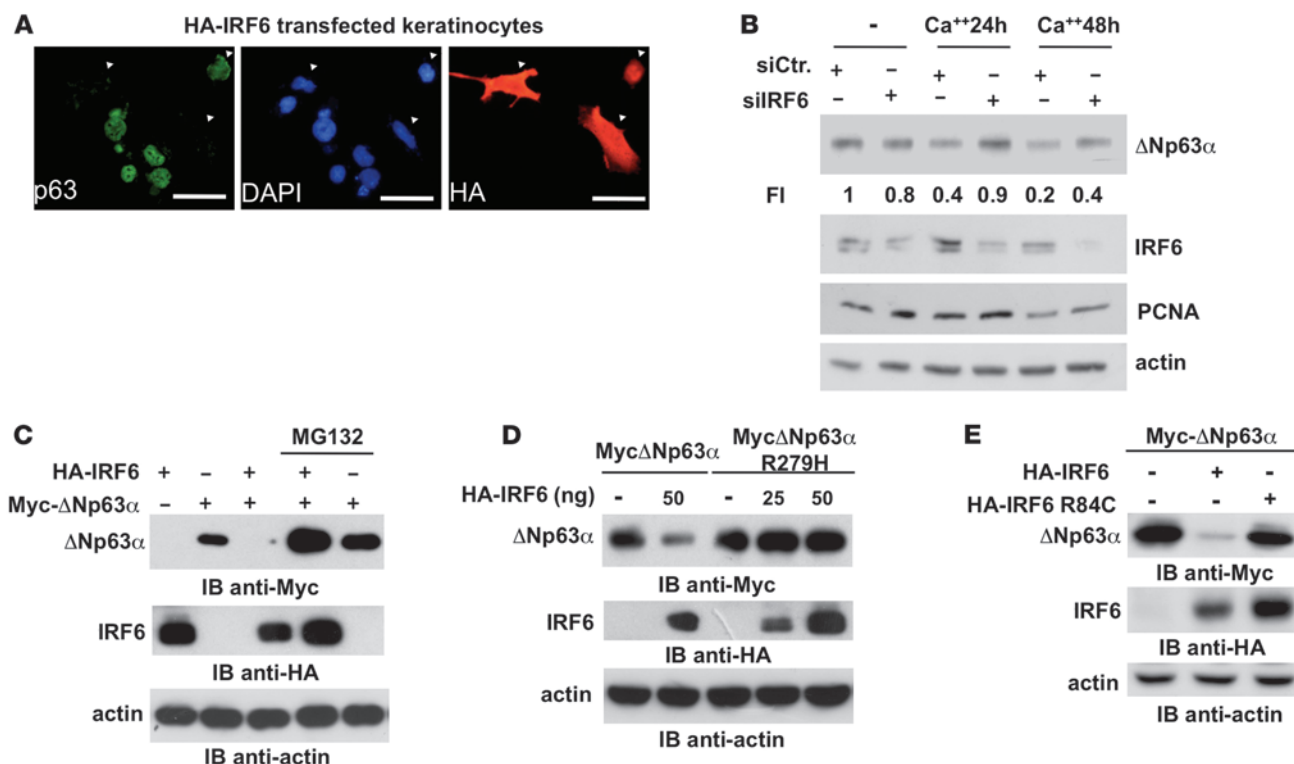
Figure 4
IRF6 induces downregulation of ΔNp63 in human primary keratinocytes. (**A**) Dual immunofluorescence on human primary keratinocytes transfected with a HA-tag–*IRF6* expression vector, with anti-HA and anti-p63 antibodies, to detect double-positive cells. Exogenous IRF6 decreased endogenous p63 expression. Arrowheads indicate transfected cells. Cell counts are reported in Table 1. Scale bar: 20 μm. (**B**) IRF6-depleted keratinocytes fail to downregulate ΔNp63 expression. Human primary keratinocytes were transfected with control (siCtr) or *IRF6*-specific (siIRF6) siRNA, followed by immunoblot detection of ΔNp63, IRF6, and PCNA. ΔNp63 was quantified by the ImageJ software, normalized, and expressed as fold induction (FI). (**C**) Immunoblot detection of HA-tag–IRF6 and ΔNp63α in U2OS cells transfected with HA-IRF6 or ΔNp63α expression plasmids and treated with the proteasome inhibitor MG132 (5 μM, 6 hours). MG132 treatment inhibited ΔNp63 downregulation by IRF6. (**D**) Immunoblot detection of ΔNp63α and IRF6 in H1299 cells transfected with a vector expressing either wild-type ΔNp63α or mutated ΔNp63α-R279H, in the presence or absence of HA-IRF6. ΔNp63α-R279H is resistant to IRF6-mediated downregulation. (**E**) Immunoblot detection of ΔNp63α and IRF6 in H1299 cells transfected with a ΔNp63α expression vector, in the presence of either wild-type or R84C mutant IRF6. The IRF6-R84C mutant failed to induce ΔNp63α downregulation. Results are representative of 3 independent experiments.

van der Woude syndrome, was unable to induce ΔNp63 downregulation (Figure 4E). This observation correlates with increased levels of p63 in the perfusion medial edge epithelia and the midline epithelial seam of Irf6-R84C knock-in mice palates (21). Thus, disease-related p63- and IRF6-mutant proteins are unable to establish a correct biochemical regulation, and we can postulate that in epithelial cells of patients affected by these mutations, the amount of ΔNp63 remains abnormally high, consequent to alteration of this regulatory pathway. Failure of p63 to be downregulated at the appropriate time may result in increased proliferation of epidermal keratinocytes or cells of the embryonic palate.

IRF6 negatively modulates the proliferative potential of epithelial cells. To establish a role for IRF6 in epithelial cell proliferation, we determined the colony-forming efficiency of epithelial cells (TE13 cells) in which IRF6 was exogenously expressed. IRF6 overexpression resulted in a marked reduction in colony formation efficiency (Figure 5A). In the same assay, coexpression of normal IRF6 with the R279H mutated ΔNp63α, resistant to IRF6-dependent degradation, restored the colony-forming efficiency to a normal level, while wild-type ΔNp63α did not (Figure 5A). These results suggest

that inhibition of epithelial cell growth requires downregulation of ΔNp63 protein, consequent to an increased *IRF6* expression, and that disease-causing *p63* mutations compromise this regulation.

To establish a role for IRF6 in the control of the proliferative potential of epidermal cells, we adopted the paradigm developed for therapeutic epidermal transplants on human epidermis, which estimates the self-renewal potential of epithelial cells via the generation of holoclones, meroclones, and paraclones in vitro (27, 28).

Table 1

Effect of IRF6 on p63 nuclear expression

Vector	HA+ p63+ cells
HA-control	84% ± 15%
HA-IRF6	36% ± 10%

Results of double staining of keratinocytes transfected with control plasmid or HA-IRF6 expressing plasmid (Figure 4A). The percentage of HA+ p63+ cells present after transfection with control and HA-tag–IRF6 is shown. Data are presented as mean ± SEM (*P* = 0.001 control vs IRF6).

A

Colony forming assay

B

C

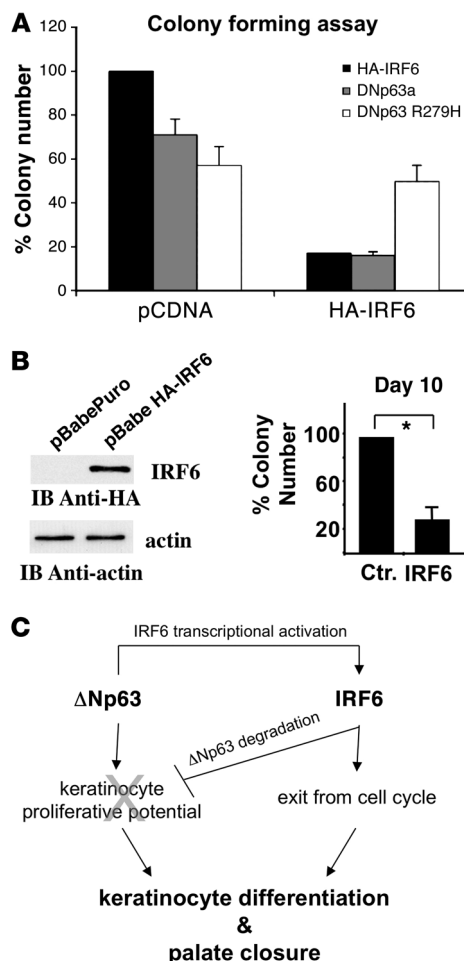**keratinocyte differentiation**
&
palate closure

Figure 5
IRF6 negatively modulates the proliferative potential of epithelial cells. (**A**) Colony formation of TE13 epithelial carcinoma cells transfected with the indicated expression vectors (ΔNp63α, ΔNp63α/R279H, or HA-IRF6). Colonies of more than 1 mm in diameter were counted, and results are expressed as mean ± SEM (3 independent experiments, duplicate samples). *IRF6* expression induced growth arrest that is partially reverted by ΔNp63α-R279H coexpression. (**B**) Colony formation of human primary keratinocytes transduced with a vector expressing HA-tag–IRF6. Immunoblotting shows HA-IRF6 expression. Actin was used as loading control. The number of colonies that were more than 1 mm in diameter was calculated with ImageJ software. IRF6 expression reduced the proliferative potential of keratinocytes. Results are expressed as percentage of each kind of colony over the total (error bars = 1 SD). $P = 0.01$, control versus IRF6 (3 independent experiments, duplicate samples). The relative percentage of holoclones, paraclones, and meroclones is shown in Table 2. (**C**) Schematic representation of the link between ΔNp63 and IRF6. *IRF6* is transcriptionally activated by ΔNp63 during differentiation. IRF6 protein expression induces ΔNp63 degradation, reducing proliferative potential of epithelial cells.

We transduced primary human keratinocytes with retroviruses expressing *IRF6* and observed that both the number and the size of clones generated by *IRF6*-expressing precursors were significantly lower than those obtained from control-infected cells (Figure 5B and Table 2). Thus, IRF6 expression reduces the proliferative potential of epidermal cells.

Discussion

IRF6 is a transcription factor, mutated in a subset of developmental syndromes, characterized by cleft lip and ectodermal dysplasia (28). The first important finding reported here is that in keratinocytes *IRF6* is a direct transcriptional target of ΔNp63 but not of TAp63. ΔNp63 maintains basal transcription levels of *IRF6* via binding to distal p63 REs (21) and is promptly recruited to the proximal p63 element upon keratinocyte differentiation stimuli. This regulation most likely takes place in epithelial cells with high proliferative potential, as ΔNp63 is the predominant isoform detectable in this compartment. Importantly, mutations in *p63*, specifically those found in patients with the EEC and AEC syndromes, strongly reduce or abolish the ability of the ΔN protein to activate *IRF6* transcription, and this correlates nicely with the reduced level of Irf6 protein expression found in the epidermis of *p63^R279H* heterozygous animals and in the epidermis of the AEC patient we examined. Together, these observations suggest that misregulation of *IRF6* expression contributes to development of the clinical phenotype of *p63*-related syndromes.

The second important finding is that, during epithelial cell differentiation, IRF6 promotes proteasome-dependent degradation of ΔNp63, thus establishing a cell-autonomous negative regulatory loop (Figure 4C and Figure 5C). During early differentiation, ΔNp63 promotes transcription of *IRF6*, and the IRF6 protein in turn promotes ΔNp63 degradation. Considering that ΔNp63 critically endows the epidermal cells with an elevated proliferation potential (7), this regulation may have the functional consequence of posing a limit to keratinocyte proliferation and allowing keratinocyte terminal differentiation and palate closure during embryonic development. Indeed, we show that increased *IRF6* expression results in lower clonogenicity and reduced proliferation of cultured epithelial cells.

Importantly, the mutant IRF6 proteins found in patients with the van der Woude syndrome are unable to bind to their cognate REs (29) and cannot induce p63 degradation. Thus, in these patients, abnormally high levels of ΔNp63 protein are retained in progenitor cells, with pathological consequences. The R279H mutant *p63* is also resistant to IRF6-mediated degradation, thus providing further evidence that the disruption or misfunctioning of the regulatory loop among these transcription factors, either resulting in hyperactivity or in hypoactivity, has pathological effects.

We propose that in normal epidermal cells the negative regulatory loop indicated by our model is initiated by ΔNp63 binding to the *Irf6* promoter and is subsequently needed for the exit of the cells from the cell-cycle and for the initiation of a tissue-specific differentiation program. Alterations in this molecular pathway are likely to affect the execution of a normal differentiation program, essential for the correct maturation and stratification of the epidermis and for the morphogenesis of structures requiring epithelial-mesenchymal interaction, such as lip/palate closure and limb bud patterning and growth.

In summary, our data highlight the importance of a developmental feedback regulatory loop between *p63* and *IRF6* for the control of proliferation of epithelial cells and link two phenotypically similar, but genetically distinct, groups of ectodermal dysplasias into one common pathway. Future studies aimed at modulating this pathway for therapeutic purposes will require

Table 2
Clone distribution at day 10

Retrovirus	Holoclones	Paraclones	Meroclones
Control	25%	42%	33%
HA-IRF6	8%	31%	61%

HA+ colonies were counted and classified according to their size and morphology as holoclones (>15 mm diameter), paraclones (<15 mm and >5 mm diameter), and meroclones (<5 mm diameter). The percentage of holoclones, paraclones, and meroclones present after exposure to either control plasmid or HA-IRF6 retroviruses is shown. Results are related to experiments shown in Figure 5B.

the identification of tissue-specific *IRF6* targets and the full comprehension of the molecular mechanisms that tightly regulate p63 stability/degradation.

Methods

Cell culture. Mouse and human primary keratinocytes were cultured as described previously. Use of mouse and human keratinocytes was approved by the University of Torino and the University of Rome "Tor Vergata" Institutional Review Boards, respectively (30). TE13 cells (epithelial SCC cell line; gift of Pierre Hainaut, International Agency for Research on Cancer, Lyon, France) and H1299 cells were cultured in RPMI medium containing 10% FBS and antibiotics (100 U/ml penicillin and 10 μg/ml streptomycin) at 37°C. To measure clonogenic growth, TE13 cells transfected with Lipofectamine (Invitrogen) were selected in G418 (600 μg/ml) (Invitrogen) for 15 days, before fixation in 4% PFA and staining with Crystal Violet. Colonies with a diameter of more than 1 mm were scored using NIH Image software (http://rsb.info.nih.gov/nih-image/). U2OS cells were cultured in DMEM containing 10% FBS and antibiotics (100 U/ml penicillin and 10 μg/ml streptomycin) at 37°C.

Plasmids, retroviruses, and TA assays. Expression plasmids encoding for Myc-tagged wild-type TA-ΔN-p63s and the ΔNp63α mutant R279H (EEC) have been reported previously (16). Human HA-tagged IRF6 expression plasmid was constructed by cloning the human *IRF6* ORF into the pCDNA-HA vector. The R84C mutation was introduced in *IRF6* by custom mutagenesis service (Biofab Research Inc.). Inserts were sequence verified.

A retroviral (pBABE-puro) expression vector with the HA-*IRF6* ORF was derived by PCR amplification from the pCDNA plasmid. Luciferase reporter plasmid and retrovirus production are described in the Supplemental Methods.

ChIP assay. For ChIP assays, mouse primary keratinocytes were used. ChIP assays were performed as described previously (20). The mouse monoclonal antibody anti-p63 (4A4) (Santa Cruz Biotechnology Inc.) or isotypic control antibodies (monoclonal anti-HA [F-7] antibody; Santa Cruz Biotechnology Inc.) were used. PCR reactions were performed for 25–35 cycles, with an annealing temperature of 55°C–57°C. Primers used in ChIP assay are indicated in the Supplemental Methods.

RNA interference. siRNA duplexes targeting ΔNp63, TAp63, and GFP, used for gene expression array (Figure 1, A and B), were obtained from MWG-Biotech. Mouse primary keratinocytes, plated on collagen-coated 35-mm dishes, were transfected with 0.5 μg siRNA per dish using Lipofectamine 2000 (Invitrogen). For experiments described in Figure 3B and in Supplemental Figure 2, we used stealth siRNAs (Invitrogen). siRNA duplexes targeting human IRF6 (catalog no. 1299003; Invitrogen) were used to knockdown *IRF6* mRNA; scrambled siRNA (Invitrogen) were used as control. Human primary keratinocytes were plated on collagen-coated 35-mm dishes and transfected with 50 nM siRNAs using Lipofectamine 2000.

GeneChip and gene expression analysis. Total RNA extracted from control and ΔNp63- and TAp63-depleted human primary keratinocytes was used to synthesize biotinylated complementary RNA (cRNA), using the GeneChip One-Cycle Target Labeling and Control Reagents kit (Affymetrix). Fifteen μg of fragmented cRNA were used for hybridization to GeneChip Mouse Genome 430 2.0 arrays (Affymetrix), for analysis of over 39,000 transcripts. Scanning and analysis were performed as described previously (28). Analysis criteria are described in the Supplemental Methods.

Immunoblotting. The following antibodies were used: monoclonal antibodies against HA (F-7) and Myc (9E10) epitopes, p63 (4A4), polyclonal antibodies against PCNA (PC10), and actin (C11) were purchased from Santa Cruz Biotechnology Inc.; anti-keratin (anti-K1) was purchased from Covance; mouse polyclonal anti-IRF6 from was purchased from Abnova Inc.; and goat polyclonal anti-IRF6 antibody (IMG3484) was purchased from Imgenex. For immunoblotting, cells were lysed in 50 mM Tris, pH 8.0, 120 mM NaCl, and 0.5% NP-40, and protein concentration was determined. Forty micrograms of total cell extract were separated by SDS-PAGE, blotted, incubated with the antibody, and developed with the ECL system (Amersham Pharmacia Biotech). The MG132 inhibitor was from Sigma-Aldrich.

mRNA expression analysis. For RT-qPCR, total RNA was extracted using TRIzoL Reagent (Invitrogen). One μg of total RNA was reverse transcribed with GeneAmp RNA PCR (Applied Biosystems). For RT-qPCR in human cells, the RT reaction products were used for real-time qPCR amplification, which was performed with the MyiQ Single-Color Real-Time Detection System (Bio-Rad). The human acidic ribosomal protein P0 (*hARP*) gene was used for normalization. Total RNA was extracted from formalin-fixed, paraffin-embedded sections using the Optimum FFPE RNA Isolation Kit (Ambion), according to the manufacturer's protocol. Primer sequences are available in the Supplemental Methods.

Immunohistochemistry and immunofluorescence. Four-mm punch biopsy specimens were taken from normal skin of healthy volunteers (*n* = 4). Declaration of Helsinki protocols were followed, and patients gave written approved consent before biopsy. Care and use of human tissues was approved by the University of Rome "Tor Vergata" Institutional Review Board. A patient affected by AEC (I537T mutation in p63) was subjected to skin biopsy on lesional skin, after obtaining informed consent from his parents. Immunofluorescence analysis was performed on 5×10^4 to 10×10^4 cells seeded on Chamber Slides (Nalge Nunc International), fixed with 4% PFA, and permeabilized with 0.2% Triton X-100. Immunohistochemistry and immunofluorescence were carried out by standard methods (Supplemental Methods).

Mouse strains and hybridization procedure. The *Brdm2* mouse strain, also designated *p63*[–] (8), that carries a null *p63* allele was genotyped by RT-PCR on embryonic RNA, with primers annealing to the C terminus of the α isoform (*Trp63*) mRNA. In mice carrying the *p63*[R279H] mutation (an EEC mutation in humans) (19), a *Bsa*HI restriction site was abrogated and was used to determine the genotype, following PCR amplification with primers flanking codon 279. The genotype was determined by PCR amplification with primers flanking codon 279, followed by digestion with *Bsa*HI. In situ hybridization was performed as described previously (31) and as described in the Supplemental Methods.

Statistics. Statistical evaluations were carried out using SigmaStat 2.03 (SPSS). For all tests, *P* values of less than 0.05 were considered significant.

Address correspondence to: Antonio Costanzo, Department of Dermatology, University of Rome "Tor Vergata," Viale Oxford 81, 00133 Rome, Italy. Phone: 39.0672596177; Fax: 39.0620902742; E-mail: antonio.costanzo@uniroma2.it.

1. Yang A, et al. p63, a p53 homolog at 3q27-29, encodes multiple products with transactivating, death-inducing, and dominant-negative activities. *Mol Cell*. 1998;2(3):305–316.
2. Yang A, et al. p63 is essential for regenerative proliferation in limb, craniofacial and epithelial development. *Nature*. 1999;398(6729):714–718.
3. Ghioni P, Bolognese F, Duijf PH, Van Bokhoven H, Mantovani R, Guerrini L. Complex transcriptional effects of p63 isoforms: identification of novel activation and repression domains. *Mol Cell Biol*. 2002;22(24):8659–8668.
4. Dohn M, Zhang S, Chen X. p63alpha and DeltaN-p63alpha can induce cell cycle arrest and apoptosis and differentially regulate p53 target genes. *Oncogene*. 2001;20(25):3193–3205.
5. Koster MI, Kim S, Roop DR. p63 deficiency: a failure of lineage commitment or stem cell maintenance? *J Investig Dermatol Symp Proc*. 2005;10(2):118–123.
6. Koster MI, et al. p63 induces key target genes required for epidermal morphogenesis. *Proc Natl Acad Sci U S A*. 2007;104(9):3255–3260.
7. Senoo M, Pinto F, Crum CP, McKeon F. p63 is essential for the proliferative potential of stem cells in stratified epithelia. *Cell*. 2007;129(3):523–536.
8. Mills AA, Zheng B, Wang XJ, Vogel H, Roop DR, Bradley A. p63 is a p53 homologue required for limb and epidermal morphogenesis. *Nature*. 1999; 398(6729):708–713.
9. van Bokhoven H, et al. p63 Gene mutations in eec syndrome, limb-mammary syndrome, and isolated split hand-split foot malformation suggest a genotype-phenotype correlation. *Am J Hum Genet*. 2001;69(3):481–492.
10. Rinne T, Brunner HG, van Bokhoven H. p63-associated disorders. *Cell Cycle*. 2007;6(3):262–268.
11. Lo Iacono N, et al. Regulation of Dlx5 and Dlx6 gene expression by p63 is involved in EEC and SHFM congenital limb defects. *Development*. 2008; 135(7):1377–1388.
12. Radoja N, et al. Homeobox gene Dlx3 is regulated by p63 during ectoderm development: relevance in the pathogenesis of ectodermal dysplasias. *Development*. 2007;134(1):13–18.
13. Lopardo T, et al. Claudin-1 is a p63 target gene with a crucial role in epithelial development. *PLoS ONE*. 2009;3(7):e2715.
14. Richardson RJ, et al. Irf6 is a key determinant of the keratinocyte proliferation-differentiation switch. *Nat Genet*. 2006;38(11):1329–1334.
15. Ingraham CR, et al. Abnormal skin, limb and craniofacial morphogenesis in mice deficient for interferon regulatory factor 6 (Irf6). *Nat Genet*. 2006;38(11):1335–1340.
16. Rahimov F, et al. Disruption of an AP-2alpha binding site in an IRF6 enhancer is associated with cleft lip. *Nat Genet*. 2008;40(11):1341–1347.
17. Kondo S, et al. Mutations in IRF6 cause Van der Woude and popliteal pterygium syndromes. *Nat Genet*. 2002;32(2):285–289.
18. Jowett AK, Vainio S, Ferguson MW, Sharpe PT, Thesleff I. Epithelial-mesenchymal interactions are required for msx 1 and msx 2 gene expression in the developing murine molar tooth. *Development*. 1993;117(2):461–470.
19. Lo Iacono N, et al. Regulation of Dlx5 and Dlx6 gene expression by p63 is involved in the EEC and SHFM congenital limb defects. *Development*. 2008;135(7):1377–1388.
20. Marinari B, et al. IKKalpha is a p63 transcriptional target involved in the pathogenesis of ectodermal dysplasias. *J Invest Dermatol*. 2009;129(1):60–69.
21. Thomason HA, et al. Cooperation between the transcription factors p63 and IRF6 is essential to prevent cleft palate in mice. *J Clin Invest*. 2010; 120(5):1561–1569.
22. Liefer KM, Koster MI, Wang XJ, Yang A, McKeon F, Roop DR. Downregulation of p63 is required for epidermal UV-B-induced apoptosis. *Cancer Res*. 2000;60(15):4016–4020.
23. Yi R, Poy MN, Stoffel M, Fuchs E. A skin microRNA promotes differentiation by repressing 'stemness'. *Nature*. 2008;452(7184):225–229.
24. Lena AM, et al. miR-203 represses 'stemness' by repressing DeltaNp63. *Cell Death Differ*. 2008; 15(7):1187–1195.
25. Li Y, Zhou Z, Chen C. WW domain-containing E3 ubiquitin protein ligase 1 targets p63 transcription factor for ubiquitin-mediated proteasomal degradation and regulates apoptosis. *Cell Death Differ*. 2008;15(12):1941–1951.
26. Westfall MD, Joyner AS, Barbieri CE, Livingstone M, Pietenpol JA. Ultraviolet radiation induces phosphorylation and ubiquitin-mediated degradation of DeltaNp63alpha. *Cell Cycle*. 2005;4(5):710–716.
27. Barrandon Y, Green H. Cell size as a determinant of the clone-forming ability of human keratinocytes. *Proc Natl Acad Sci U S A*. 1985;82(16):5390–5394.
28. De Luca M, Pellegrini G, Green H. Regeneration of squamous epithelium from stem cells of cultured grafts. *Regen Med*. 2006;1(1):45–57.
29. Little HJ, et al. Mis-sense mutations that cause Van der Woude syndrome and popliteal pterygium syndrome affect the DNA-binding and transcriptional activation functions of IRF6. *Hum Mol Genet*. 2009;18(3):535–545.
30. Marinari B, et al. The tumor suppressor activity of IKKalpha in stratified epithelia is exerted in part via the TGF-beta antiproliferative pathway. *Proc Natl Acad Sci U S A*. 2008;105(44):17091–17096.
31. Levi G, et al. Msx1 and Dlx5 act independently in development of craniofacial skeleton, but converge on the regulation of Bmp signaling in palate formation. *Mech Dev*. 2006;123(1):3–16.